DESY 95-142
July 1995

Virtual Pion Scattering at HERA

G. Levman
Department of Physics, University of Toronto, Ontario, Canada

K. Furutani
Department of Physics, York University, Toronto, Ontario, Canada

ISSN 0418-9833

DESY 95-142
July 1995

ISSN 0418-9833

Virtual Pion Scattering at HERA

G. Levman*
Department of Physics, University of Toronto, Toronto, Ontario M5S 1A7

K. Furutani
Department of Physics, York University, Toronto, Ontario M3J 1P3

July 11, 1995

Inclusive neutron and Δ^{++} production has been studied extensively in low energy hadron-hadron collisions. Experiments show that the cross section for small momentum transfers is dominated by one pion exchange (OPE). By examining the system recoiling from the produced neutron or Δ^{++} virtual pion-nucleon interactions can be investigated. In low Q^2 interactions at HERA the production of a leading neutron or Δ^{++} is also dominated by OPE and virtual $\gamma\pi$ collisions can the studied. The total $\gamma\pi$ cross section can be measured as well as the photoproduction of jets from pions. If OPE is also an important component of deep inelastic scattering, virtual $e\pi$ collisions can be investigated, and structure functions of the pion extracted in both neutral and charged current interactions. A forward neutron calorimeter and a leading proton spectrometer detect leading baryons, in effect supplying the experiments with a tagged pion beam. In this paper we review experimental and theoretical aspects of one pion exchange. We estimate cross sections for virtual pion scattering at HERA. We examine some expected characteristics of the final state of the virtual $e\pi$ events.

1 Introduction

In hadron-hadron collisions target fragmentation has been subjected to much investigation both at Fermilab and at CERN. In particular, using pion and proton beams, inclusive proton (neutron) production has been measured from

target neutrons (protons), and inclusive Δ^{++} production from protons. These studies show that inclusive charge exchange reactions in hadron-nucleon scattering display two remarkable properties: the factorization of the cross section and the dominance of one pion exchange. The processes $p \to n$ and $p \to \Delta^{++}$ proceed independently of the beam particle, and the inclusive cross section factorizes into the product of a virtual pion flux and a pion total cross section (Fig. 1).

When a photon interacts like a hadron it behaves very much like a vector meson. As a result, we expect factorization and OPE to make an important contribution to the photoproduction of leading baryons. In particular this should be true at HERA, provided the virtuality of the exchanged photon, Q^2, is small, $Q^2 \leq \mathcal{O}(m_\rho^2)$, the mass squared of the ρ meson.

In deep inelastic scattering (DIS) the situation is less clear. On theoretical grounds, one pion exchange is expected to make important contributions to the inclusive structure functions of nucleons[1, 2] and nuclei[3, 4]. And pion cloud effects can explain the excess of $\overline{d}$ quarks over $\overline{u}$ quarks in the proton[5, 6]. The interactions $ep \to [e, \nu][n, \Delta^{++}]X$ where the n or Δ^{++} is fast, isolate the target fragmentation region of phase space where the OPE contribution is most important (Fig. 2). At HERA the energy of the virtual pion beam is considerable, and one obtains $\gamma\pi$ and $e\pi$ scattering energies comparable to those achieved in experiments at Fermilab and CERN. Both factorization and OPE can be checked at HERA, and their dependence on Q^2 and x studied, if the relevant events are tagged.

The cleanest and most direct method is the detection of the leading particle itself. This allows the measurement of kinematical variables in addition to those provided by the electron alone. For the neutron one needs a calorimeter at zero degrees; for the Δ^{++}, a leading particle spectrometer with multi-track capability to detect the products of the $\Delta^{++} \to p\pi^+$ decay. The ZEUS experiment has a leading proton spectrometer. It has recently installed a forward neutron calorimeter, and some preliminary results have already been reported[7, 8].

In hadron interactions, virtual pion scattering has been employed to examine the properties of meson-pion and proton-pion collisions. Corresponding studies are possible at HERA. Good measurements will yield important information on the parton structure of the pion and on photon-pion interactions at high energies.

Structure functions are model independent quantities which can be mea-

sured directly only in deep inelastic lepton scattering. Once these functions are known, parton densities can be determined from them. Parton densities can also be obtained from hadron collision data. At present the parton densities in the pion are only poorly determined by experiment using jet production, J/Ψ production, or the Drell-Yan process in pion-nucleon interactions. The need to unfold the nucleon parton densities greatly increases the uncertainties in the determination. Also the Q^2 scale at which the densities are extracted is timelike rather than spacelike. These problems would be circumvented if the pion were studied in deep inelastic electron scattering. Structure functions would be measured directly and unambiguously.

In photoproduction, the total $\gamma\pi$ cross section can be determined in a manner identical to the measurement of the total γp cross section. Both soft and hard photon induced processes can be studied. In particular, jet production will cast new light on the nature of the constituents of the photon and pion.

These measurements are analogous, and complementary, to the proposed measurement of the structure function of the pomeron, through the study of the reaction $ep \to epX$[9, 10]. This reaction most likely dominates the sample of large rapidity gap events observed first by the ZEUS collaboration[11]; whatever our ultimate understanding of these events, the experimental and theoretical interpretation of the data would be greatly assisted by data samples with tagged proton and tagged neutron events[12, 13, 14].

In this paper we review briefly some important experimental evidence for factorization (Section 2) and one pion exchange (Section 3). We review the theoretical formalism and estimate the virtual pion flux at HERA and the cross sections for deep inelastic virtual $e\pi$ scattering (Section 4). We study some general characteristics of final states using the Monte Carlo program HERWIG[15], which we have modified to include virtual pion scattering (Section 5).

2 Factorization

In the study of single particle inclusive reactions, $ab \to cX$, experiments restrict themselves, either by design or by cuts on data, to the analysis of only one outgoing particle. As the Mandelstam diagram shown in Fig. 1 illustrates, the cross section is determined by only three independent kine-

matical variables: s the center of momentum system (cms) energy squared, $t = (p - p')^2$ the momentum transfer squared for $b \to c$, and M_X^2, the invariant mass squared of the recoiling system X. Under the hypothesis that the amplitude for the process factorizes, the resulting Feynman diagram has two vertices connected by an exchanged particle, or, more generally, by a Regge trajectory or reggeon, d. One vertex consists of the transition $b \to c$; the other of the interaction $ad \to X$. The Lorentz invariant differential cross section for the inclusive interaction may be written now as[16, 17]

$$\frac{d^2\sigma}{dtdz} = f_{d/b}(t, z)\sigma_{ad}(M_X^2, t), \tag{1}$$

where $f_{d/b}$ is interpreted as the flux of virtual particles d carrying the momentum fraction $z = M_X^2/s$ of b; and σ_{ad} is the total cross section for $ad \to X$ at cms energy squared M_X^2.

At Fermilab, the charge exchange reactions $p \to \Delta^{++}$ and $n \to p$ (or $p \to n$ by isospin symmetry) have been studied using secondary hadron beams, $\pi^{\pm}/p$, incident on the 30 in. bubble chamber, and also using an internal gas jet in the main accelerator. The beam energies have ranged from 50 to 400 GeV so there is much data for tests of factorization and the additional expectation that the process is dominated by pion exchange[18]. The data occupy essentially the same restricted region of the final state phase space, that is, the beam fragmentation region, where $|t|$ is small (< 1 GeV^2). As a result, the dependence of σ_{ad} on t is small. In addition, since high energy total cross sections vary only slowly with energy, the M_X^2 dependence of σ_{ad} can often be ignored.

We begin with the bubble chamber data where proton production has been studied with p and π^+ incident on deuterium in the 30 in. bubble chamber at Fermilab[19, 20]. With a 100 GeV unseparated beam Hanlon et al. determined the ratio

$$R = \frac{d\sigma(\pi^+ n \to pX)/dM_X^2}{d\sigma(pn \to pX)/dM_X^2} \tag{2}$$

which is a measure of $\sigma(\pi^+\pi^-)/\sigma(\pi^- p)$. It proved to be independent of M_X^2 to within the experimental errors. in agreement with the slow variation with energy expected of the cross section; moreover, both the additive quark rule[21],

$$\sigma(ab) = n(a)n(b)\sigma(qq) \tag{3}$$

where $n(a)$ is the number of valence quarks in a, and the geometric scaling of cross sections,

$$\sigma(ab) = \sigma(ac)\frac{\sigma(bc)}{\sigma(cc)}, \tag{4}$$

predict that $R \approx 0.62 - 0.66$. The experiment obtained the average value $\overline{R} = 0.68 \pm 0.06$ in agreement.

At 100 GeV the total cross section for $pn \rightarrow pX$ for $|t| < 1$ GeV^2 was determined to be 5.7±0.3 mb. Hartner[20], in his unpublished thesis, studied the same reaction but with a beam energy of 200 GeV. He obtained a cross section of 6.34±0.21 mb for $|t| < 1.4$ GeV^2. Adjusting this cross section using his measured t distribution, we obtain the result 5.5±0.3 mb for $|t| < 1$ GeV^2, in good agreement with the 100 GeV result.

Inclusive Δ^{++} production has been studied with $\pi^{\pm}$ and p beams incident on hydrogen. Beam energies have varied from 100 to 360 GeV, so there is a good mix of data for studying both beam and energy dependent effects[22, 23, 24, 25, 26]. The interpretation of the different experiments is complicated by the use of different methods for extracting the Δ signal from the double inclusive $p\pi^+$ data. The methods vary from fitting line shapes[23, 24] to simply counting events above a smooth hand-drawn background curve[26, 25]. Also, different groups apply different t and p_T cuts to their data before quoting cross sections or attempting fits.

The normalization uncertainties are clearly shown in a comparison of Δ^{++} production in $\pi^- p$ interactions at beam energies of 100, 200, and 360 GeV[24]. The authors fit the $p\pi^+$ mass distribution to a relativistic p-wave Breit-Wigner. Depending on the form of background term they find cross sections that varied by up to 50%. In contrast, an s-wave Breit-Wigner gave cross sections 10%-20% lower[23]. Nevertheless, a study of these results shows that there is no indication of variation with energy in the data, once a consistent method of extraction of the Δ^{++} signal is chosen.

Data for pp interactions is available at 100, 200 and 303 GeV, but studied by different groups[22, 25, 26]. The 100 GeV data has a $|t| < 0.88$ GeV^2, in contrast to the 200 and 303 GeV data for which $|t| < 1.0$ GeV^2. In order to compare cross sections the 100 GeV value must be adjusted up by 10%±1%, as determined from the measured t distributions in the π^- and p data. After this is done we conclude that here too the data is consistent with little energy variation.

	$n \xrightarrow{\pi^+} p$ [19]	$n \xrightarrow{p} p$ [27]	$p \xrightarrow{p} \Delta^{++}$ [28]	$p \xrightarrow{\pi^+} \Delta^{++}$ [29]	$p \xrightarrow{\pi^-} \Delta^{++}$ [30]
σ (mb)	3.9±0.3	5.6±0.2	1.47±0.10	1.16±0.16	0.91±0.05

Table 1: Cross sections for inclusive n and Δ^{++} production. The particle above the arrow is the second beam particle. Columns 1-5 correspond to Eqns. 5-9, respectively.

A summary of the total inclusive cross sections for both neutron and Δ^{++} production with $|t| < 1$ GeV^2 is given in Table 1. The cross sections have been adjusted for any difference in t range. In addition, because there is no indication of any energy dependence, and in order to reduce normalization differences, we have averaged the cross sections measured at different beam energies. We now neglect any t and M_X^2 dependence of total cross sections σ_{ad} and integrate Eqn. 1 to obtain:

$$\sigma(\pi^+ n \to pX) = \sigma(\pi^-\pi^+) f_{\pi^+/p} \quad (5)$$

$$\sigma(pn \to pX) = \sigma(\pi^- p) f_{\pi^+/p} \quad (6)$$

$$\sigma(pp \to \Delta^{++} X) = \sigma(\pi^- p) f_{\pi^-/p} \quad (7)$$

$$\sigma(\pi^+ p \to \Delta^{++} X) = \sigma(\pi^-\pi^+) f_{\pi^-/p} \quad (8)$$

$$\sigma(\pi^- p \to \Delta^{++} X) = \sigma(\pi^-\pi^-) f_{\pi^-/p}. \quad (9)$$

We can estimate $\sigma(\pi^-\pi^-)/\sigma(\pi^-\pi^+)$, $\sigma(\pi^-\pi^+)/\sigma(\pi^- p)$ and the flux factor ratio f_{π^+}/f_{π^-} by taking appropriate ratios of measured cross sections. The Pomeranchuk theorem predicts that $\sigma(\pi^-\pi^-) \approx \sigma(\pi^-\pi^+)$; however, at Fermilab energies we expect instead that $\sigma(\pi^-\pi^-) \leq \sigma(\pi^-\pi^+)$ since the reaction $\pi^-\pi^+ \to X$ has annihilation channels which are missing in $\pi^-\pi^-$ collisions. The use of Table 1 gives $\sigma(\pi^-\pi^-)/\sigma(\pi^-\pi^+) = 0.78 \pm 0.12$. For the ratio $\sigma(\pi^-\pi^+)/\sigma(\pi^- p)$ we obtain the values 0.70 ± 0.06 and 0.79 ± 0.12. Since these last two agree to within errors, they have been averaged in obtaining the following six values for the flux factor ratio:

$$\frac{f_{\pi^+}}{f_{\pi^-}} = 3.7,\ 3.4,\ 3.3,\ 3.8,\ 3.5,\ 3.4 \quad (10)$$

with an average of 3.5. For completeness we also note the data in the table imply $\sigma(\pi^-\pi^-)/\sigma(\pi^-p) = 0.66 \pm 0.08$, in agreement with quark counting rules.

The $t' = t - t_{min}$ and z distributions can be compared as well. In this respect, the pp and $\pi^-p \to \Delta^{++}X$ data for 200 GeV show the same behavior[25, 24]. Both reactions have exponential t' distributions with a slope parameter of about 8 GeV^{-2}. The z distributions show the same rapid rise, broad maximum centered at $z = 0.1$, and gentle fall off.

Taken altogether, these results show that the data are in good agreement with the hypothesis of factorization and have, at most, a weak energy dependence. Knowledge of the cross sections for one type of beam at one energy can be used to predict the results for other beams at other energies.

3 One Pion Exchange

The hypothesis of factorization, by itself, does not give us an expression for the flux factors. For that, additional assumptions are needed. If pion exchange is dominant at the target vertex, then the flux factor can be written[18, 31, 33]

$$f_{\pi/p} = \frac{1}{4\pi}\frac{G^2}{4\pi}\frac{V(t)}{(m_\pi^2 - t)^2} z^{1-2\alpha_\pi(t)} F(t,z). \tag{11}$$

The various factors in this formula have simple interpretations. The denominator $m_\pi^2 - t$ is the pion propagator; z^1, the pion's momentum fraction, is also the ratio of virtual to real beam fluxes. The exponent of z, $\alpha_\pi(t) = \alpha'_\pi(t - m_\pi^2)$, the pion's Regge trajectory, is important only at large t, and is often omitted ($\alpha'_\pi = 0$) for simplicity. Other Regge terms may also be present but their contribution is expected to be important only at large z and $|t|$[16]. The function $F(t,z)$ is a form factor introduced to account for off-mass-shell and absorptive effects. When the pion trajectory is retained in Eqn. 11, $F(t,z)$ is usually assumed to be a simple exponential[16, 18]:

$$F(t) = e^{b(t-m_\pi^2)}; \tag{12}$$

when omitted, an exponential with a z dependence:

$$F(t,z) = e^{b(t-m_\pi^2)/z}. \tag{13}$$

In the latter case, the exponent of e is proportional to $M_{n\pi}^2 - M_n^2$, where $M_{n\pi}$ is the invariant mass of the $n\pi$ system and M_n is the mass of the neutron[32, 33]. The vertex functions, which express the spin and parity dependence of the pion-baryon vertex are

$$V_n(t) = -t \tag{14}$$

$$V_\Delta(t) = \frac{2}{3}\frac{[(M_\Delta + M_p)^2 - t]^2[(M_\Delta - M_p)^2 - t]}{4M_\Delta^2} \tag{15}$$

for the case of n and Δ^{++} production, respectively[18, 31]. G is the $p\pi[n, \Delta]$ coupling constant; from isospin symmetry $G_{p\pi n} = \sqrt{2}G_{p\pi p}$. In addition we set $G_{p\pi\Delta} = G_{p\pi p}$ which is close to the value obtained from the decay of the Δ^{++}. Note that $G_{p\pi p}$ is dimensionless whereas $G_{p\pi\Delta}$ has units of GeV^{-1}.

Robinson et al.[34] compared the result of their gas jet studies at Fermilab to the predictions of the OPE formula. Over the large s range, but limited z and t range spanned by the data, the model works surprisingly well considering the simplicity of the ingredients which enter into it. For the coupling constant the authors took $G_{p\pi p}^2/4\pi = 15$ as determined by low energy data[37], and they simply set $\alpha_\pi' = 1$. In addition, the πp cross section is needed for which they took the simple parameterization $\sigma_{\pi p}(M_X) = (20 + 21/M_X)$ mb[16]. After adjusting the model for Fermi motion of the target neutron in deuterium, and for possible rescattering effects the authors obtained good agreement with their data. They concluded that the data require $b = 0$ ($F(t) = 1$), otherwise the cross section is too greatly suppressed and additional terms would be needed.

Leading neutrons have also been studied at CERN with an internal target in the PS[35] and at the ISR[36]. Although the low energy data show evidence of OPE they are not well described by the models. On the other hand, for the ISR data, the pion Regge trajectory is in good agreement with the effective trajectory determined by the experimenters.

OPE has also been studied over a larger t range in inclusive proton production with 100 and 200 GeV p on deuterium[22, 20]. These experiments also found that the simple model described above agreed very well with the $pn \to pX$ data. Hartner's results, which cover the greatest range in $|t|(< 1.4\ \mathrm{GeV}^2)$, are shown in Figs. 3 and 4. The curves are the predictions of Eqn. 11 adjusted for deuterium as described above. Hartner concludes "the agreement is remarkable because no parameters were used for fitting,

and because agreement in the higher M_X^2 region occurs where one of the triple-Regge limits (s/M_X^2 large) is not even satisfied'. Because of the good general agreement of data and OPE, Erwin et al. were able to extract the $\pi^-\pi^+$ total cross section from their $\pi^+p \to nX$ data.

Compared to neutron production, the situation for Δ^{++} production is less satisfactory, not only for the experimental reasons discussed above, but also because of theoretical uncertainties which include the greater role played by absorptive effects when a resonance is excited[38, 39]. The presence of such effects in Δ^{++} production can be studied through the measurement of the density matrix elements of its decay to $p\pi^+$[40]. The experimental results show good consistency and demonstrate the importance of absorptive effects.

The authors of the π^-p compilation[24] combined their data which were at different energies to study the OPE formalism. They made no attempt to study the vertex factor V_Δ, but instead divided the data into t bins and fit the M_X^2 distributions to determine the exchanged trajectory. The result was in excellent agreement with pion trajectory dominance.

In the pp data[25] there is an excess of events at low z. By imposing a slope parameter of $b = 6$ GeV^{-2}, good agreement was found, but at the cost of introducing a rather severe $p_T^2 < 0.1$ GeV^2 cut on the data. In contrast, Goldstein and Owens[39] found good agreement using a simple pole model (no absorptive corrections) with $b = 1.5$ provided the coupling constant $G^2_{p\pi\Delta}/4\pi$ was reduced by almost 50%. On the other hand, in a model which included absorptive effects, they obtained good agreement with the data, this time keeping the coupling constant fixed at its nominal value ≈ 18, as determined by the width of the Δ^{++}[37, 31]. In all cases the presence of additional Regge terms was required.

In principle, the neutron and the Δ can also be produced by pomeron exchange from the diffractive dissociation of the incoming proton; however, all the inclusive data is consistent with the hypothesis that OPE is the dominant mechanism in charge exchange reactions. Hartner, for instance, searched his data for N^* production as a background for OPE, but could only set an upper limit[20].

4 Cross Sections for ep scattering

The discussion in the previous section shows that for hadron-hadron collisions factorization and OPE hold to a very good approximation in the target fragmentation region of phase space. This justifies the assumption that factoriztion and OPE will also work well in γp and ep collisions as shown in Fig. 2. If l, l', p and p' are the initial and final 4-momenta of the lepton and baryon, then the momenta of the exchanged photon and pion are $q = l - l'$ and $k = p - p'$. The 4-fold differential cross section for the two-particle inclusive reaction $ep \to e[n, \Delta^{++}]X$ can be written

$$\frac{d^4\sigma}{dtdzdydQ^2} = f_{\pi/p}(t,z)\frac{d^2\sigma^{e\pi - e'X}}{dydQ^2}(y, Q^2, t, zs) \tag{16}$$

with a similar expression for $ep \to \nu[n, \Delta^{++}]X$. The kinematical Lorentz invariants are defined as

$$z = \frac{l\cdot k}{l\cdot p} \simeq \frac{2l\cdot(p-p')}{s} \simeq \frac{E_\pi}{E_p} \simeq 1 - x_L \tag{17}$$

$$t = k^2 = (p-p')^2 \simeq -\frac{p_T^2}{1-z} \tag{18}$$

$$y = \frac{p\cdot q}{p\cdot l} \simeq \frac{2p\cdot(l-l')}{s} \tag{19}$$

$$Q^2 = -q^2 = -(l-l')^2 \tag{20}$$

$$x = x_{e\pi} = \frac{Q^2}{2k\cdot q} \simeq \frac{Q^2}{zsy} \simeq \frac{x_{BJ}}{z}. \tag{21}$$

The variables z and t are baryonic versions of the leptonic y and Q^2. The cms energy squared of the ep system is $s = (l+p)^2$. It is related to the cms energy squared of the $e\pi$ system by

$$s_{e\pi} = (l+k)^2 = m_e^2 + t + z(s - m_p^2 - m_e^2) \simeq zs. \tag{22}$$

The invariant mass of the restricted hadronic system X, that is, the hadronic system without the leading baryon, is

$$M_X^2 = (q+k)^2 = Q^2(1-x)/x + t \simeq -Q^2 + t + zys. \tag{23}$$

The flux factor,

$$f_{\pi/p}(t,z) = \frac{1}{\sigma_\pi}\frac{d^2\sigma^{p\to n,\Delta}}{dtdz}, \tag{24}$$

can be obtained either from hadron scattering data or from theory. For the present study we restrict ourselves to the use of the OPE formula, Eqn. 11.

Just as for ep scattering, the $e\pi$ cross section can be written

$$\frac{d^2\sigma^{e\pi\to eX}}{dydQ^2} = \frac{\alpha}{2\pi yQ^2}\{[1+(1-y)^2]\sigma_T^{\gamma\pi}(y,Q^2,t)+2(1-y)\sigma_L^{\gamma\pi}(y,Q^2,t)\}, \tag{25}$$

where σ_T and σ_L are the transverse and longitudinal cross sections for virtual $\gamma\pi$ scattering. These cross sections depend upon t to account for the virtuality of the exchanged pion. In the limit $Q^2 \to 0$, σ_L vanishes and σ_T becomes equal to the real total $\gamma\pi$ cross section.

The ZEUS and H1 experiments at HERA measure the total γp cross section by selecting events with an electron scattered at a small angle into the luminosity monitor[41, 42]. They have also studied jets in photoproduction[43]. In an experiment which also detects a high momentum neutron or Δ^{++} the same procedure can be implemented for $\gamma\pi$ collisions.

Deep inelastic $e\pi$ reactions have both neutral $e\pi \to eX$ and charged $e\pi \to \nu X$ current components. The neutral current cross section is

$$\frac{d^2\sigma^{e\pi\to eX}}{dxdQ^2} = \frac{2\pi\alpha^2}{xQ^4}\{[1+(1-y)^2]F_2^\pi(x,Q^2,t) - y^2F_L^\pi(x,Q^2,t)\}, \tag{26}$$

where the structure functions again depend upon t. Factorization of the ep cross section implies that the ep structure functions[13, 14] $F_2^{p\to n}$ and $F_L^{p\to n}$ for high energy neutron production $p \to n$ also factorize:

$$F_2^{p\to n}(x_{BJ},Q^2,z,t) = f(z,t)F_2^\pi(x_{BJ}/z,Q^2,t) \tag{27}$$

$$F_L^{p\to n}(x_{BJ},Q^2,z,t) = f(z,t)F_L^\pi(x_{BJ}/z,Q^2,t). \tag{28}$$

Eqn. 26 excludes Z^0 effects which are important only at the highest values of Q^2; however, they have been included in the calculations which follow. Similar expressions can be written for Δ^{++} production and for the charged current interaction.

In contrast to deep inelastic scattering at fixed cms energy s, since the virtual pions have varying energy, x, y, and Q^2 are no longer dependent

	$\sigma(ep \to)$		
	nX	$\Delta^{++}X$	X
Photoproduction	0.8 μb	0.2 μb	5.2 μb
Deep inelastic NC	12.9 nb	3.7 nb	73 nb
Deep inelastic CC	9 pb	3 pb	73 pb

Table 2: Cross sections for $ep \to [e,\nu][n,\Delta^{++}]X$ integrated over $|t| < 1$ GeV^2, $z < 0.8$. For photoproduction $10^{-7} < Q^2 < 2 \cdot 10^{-2}$ GeV^2 and $0.2 < y < 0.8$ while for deep inelastic scattering $Q^2 > 10$ GeV^2. The n to Δ^{++} cross section ratio is fixed at 3.5:1.

variables. Therefore, F_2^π and F_L^π can be individually determined using the different y dependences, at fixed x and Q^2, of the two terms in Eqn. 26; also, given sufficient data, the structure functions can be determined as a function of t and the results extrapolated to $t = m_\pi^2$ to determine on-mass-shell values.

In order to estimate cross sections at HERA we have carried out a Monte Carlo integration. We define the photoproduction kinematic regime as $10^{-7} < Q^2 < 2 \cdot 10^{-2}$ GeV^2, $0.2 < y < 0.8$, and the deep inelastic regime as $Q^2 > 10$ GeV^2. For photoproduction we have assumed ρ dominance[44] and have estimated σ_T and σ_L using geometrical scaling of cross sections (Eqn. 4) and with the total cross section parameterizations of Donnachie and Landshoff[45]. For deep inelastic scattering we have used the pion[46] and proton[47] structure function parameterizations of Owens. In both cases we take the exchanged pion on the mass shell. We have used a relativistic Breit-Wigner function to define the line shape of the Δ^{++}. For the decay we have taken density matrix elements $\rho_{33} = 0.12$ and $\rho_{31} = \rho_{3-1} = 0$, in agreement with absorptive OPE[48] and the bubble chamber data. We use the OPE flux with the pion trajectory retained and with the form factor omitted, that is, we set $\alpha'_\pi = 0$ and $F(t,z) = 1$.

We study the cross section at nominal HERA conditions of 30 GeV electrons incident on 820 GeV protons. The total integrated cross sections for $|t| < 1$ GeV^2, $z < 0.8$ are given in Table 2. The flux factor ratio $f_{\pi^+}/f_{\pi^-} = 3.5$ has been used to fix the Δ^{++} cross sections relative to those of the neutron, as described in Section 2. The data of Table 1 show that fast neutron and

Δ^{++} production form 15%-20% of the total cross section in hadron-proton collisions. The same ratio is expected in ep collisions because of factorization. For comparison, the corresponding cross sections for $ep \rightarrow [e,\nu]X$ are also given in Table 2.

Fig. 5 shows the ratio of leading neutron DIS events to all DIS events as a function of Q^2 and W, the rest mass of the hadronic system (including the neutron) recoiling from the electron. The ratio is nearly flat in both these variables. The ZEUS collaboration has observed a similar result for large rapidity gap events[11]. In view of Fig. 5, this observation can not be taken as evidence for pomeron exchange[12]. Since the scaling violations of F_2 should be similar for all hadrons, including the proton, the pion and the pomeron (provided it is composed of quarks and gluons) we should expect a weak Q^2 dependence. The W dependence is also small because hadronic collisions in general show similar energy dependences.

The differential cross sections $d\sigma/dz$ for leading neutron DIS events are shown in Fig. 6. The energy of the virtual pion beam is quite high. Since, in neutral current interactions, $\overline{z} = 0.35$ for n and $\overline{z} = 0.23$ for Δ, the experiments at HERA obtain virtual $e\pi$ collisions with an effective $\sqrt{s_{e\pi}}$ in the range 150-185 GeV. Also evident is that the z distribution for charged current interactions is harder than for neutral current interactions; this occurs because the charge current cross section is rising with energy.

It should be noted that both y and Q^2 are determined by the final state, exactly as usual for ep scattering; however, Bjorken's $x_{BJ} = Q^2/2p \cdot q$ no longer is the parton momentum fraction, x, which has an additional factor z in the denominator of its definition, $x_{e\pi} = x_{BJ}/z$. Thus a simple application of the usual definition will underestimate x. If neither the leading neutron nor Δ can be tagged, these events will complicate the analysis of the low x sample of ep scattering events. They must be included in the event sample for the determination of the proton's structure functions at low x, but perhaps they should be removed in a search for novel low x phenomena such as hot spots, or violations of the QCD evolution equation[49]. The bias introduced by ignoring the factor z is evident in the scatter plot of x_{BJ} vs $x_{e\pi}$ presented in Fig. 7.

In order to fully reconstruct the event kinematics, the produced n or Δ must be detected. They appear at low t, and moderate z. In the laboratory they are at high momentum and at very small angles with respect to the beam. Fig. 8 shows the integrated angular spectrum of neutrons. Because

of factorization there is little difference between neutral and charged current interactions. About 80% of the neutrons are produced at angles less than 1 mr. In order to detect these neutrons a calorimeter is needed which views the ep intersection point at zero degrees. The acceptance of such a calorimeter is sharply limited by magnetic elements of the beam line; however, because the production angle is so small, the angular acceptance of the calorimeter need not be large. Even for $\theta_n < 0.5$ mr, the acceptance would still be 40%. Since, on the average, the neutron carries away 65% of the beam energy, the study of the neutron spectrum requires a calorimeter with only modest energy resolution, $\delta E/E \sim 100\%/\sqrt{E}$; however, the determination of E_π involves the subtraction $E_p - E_n$. If data close to the kinematical end point is to be useful, then the calorimeter's resolution should be as good as possible. To measure $t \simeq -E_p E_n \theta_n^2$ in addition, the position of the shower must be determined. Since the calorimeter would be situated in the HERA tunnel about 100 m from the intersection point, the entrance point of the a neutron produced at $\theta_n = 0.5$ mr will reach out only 5 cm. So one needs position resolution $\mathcal{O}$(mm). The measurement of t, however, is useful, but absolutely necessary for the extraction of the structure functions, provided one is willing to ignore small off-mass-shell effects.

The measured z distribution of leading neutrons is relatively undistorted by geometric acceptance effects; in contrast, the t is strongly effected by the angular acceptance of a zero degree calorimeter. Fig. 9 shows $d\sigma/dt$ both before and after an angle cut of $\theta_n < 0.5$ mr. The distribution vanishes at $t = 0$ because of the pseudoscalar nature of the vertex function (Eqn. 14), but it rises quickly and peaks near $t = -0.15$ GeV^2. The angular restriction strongly depletes the distribution above the peak. This is an advantage because other particle exchanges besides the π, such as the ρ, become increasingly important at larger $|t|$[33].

The experimental acceptance for the Δ^{++} is determined by the ability of the leading particle spectrometer to detect both the p and π^+ produced in the decay of the resonance. Since the kinetic energy released in the decay is small, the proton takes, on the average, 70% of the energy. For good acceptance, a leading particle spectrometer must cover a large region of x_L space and have multi-track capability. The ZEUS collaboration has such a device operating at HERA[50].

At this point it should be emphasized that the detection of the neutron is cleaner both experimentally and theoretically. The neutron cross section

is three and a half times larger than that of the Δ^{++}. Also, the acceptance for the neutron is much greater since only one particle need be detected. Finally, Δ^{++} production suffers from theoretical uncertainties because of nonresonant $p\pi^+$ production and the need for large absorptive corrections in the production of the resonance itself.

We note finally that there are tentative plans at HERA to accelerate deuterons. Should this happen, charge exchange can be studied in the reaction $ed \to [e,\nu]pXp_s$ where both the scattered proton from $n \to p$ and the spectator proton p_s are detected in a leading particle spectrometer. This would be an interesting adjunct to proton beams. The tagging of spectator neutrons n_s in deuteron interactions requires a leading neutron calorimeter. With both a zero degree calorimeter and a leading particle spectrometer all the reactions

$$ed \to [e,\nu][Xp_s, Xn_s, pXp_s, nXn_s] \tag{29}$$

become accessible to an experiment[51].

5 Properties of the final state

Until now we have presented results which follow only from consideration of the two-particle inclusive cross section. In order go further and study the properties of final states, hadronization models are required. For deep inelastic scattering the quark-parton model can be used; however, in the photoproduction regime only a small part of the cross section is expected to be due to constituent scattering. Instead, most will be due to soft processes requiring a treatment similar in spirit to the vector meson model.

Here we restrict ourselves to a brief discussion of the final states in neutral current interactions. For this purpose we used the program HERWIG to generate the final state in $e\pi$ scattering using its usual scheme of parton showering and cluster hadronization[15]. This allows us to study particle multiplicities and rapidities, and energy flows. We present only results for the reaction $ep \to enX$, Δ production being similar. For comparison, we also present the corresponding plots for the reaction $ep \to eX$ as generated by the standard approach. In principle, $ep \to eX$ contains both leading n and leading Δ^{++} reactions. In fact, we define for $ep \to eX$ the leading nucleon as one with the largest value of x_L. With this definition we find that 21% of the standard DIS events contain a leading neutron with $0 < z < 0.8$ and

$|t| < 1$ GeV^2. This is somewhat larger than the expected fraction of events according to OPE; in addition, the z and t distributions are in disagreement with OPE.

Fig. 10 shows the charged multiplicity distribution. HERWIG predicts that the most probable multiplicity in ep scattering is 4 with the average of 10.2 and a width of 8. Although the distribution for $e\pi$ is similar, it peaks higher, at 6, but has a smaller average (9.3) and width (6). The higher peak value may reflect the fact that a baryon need not be produced in the final state; the lower average and width, the reduced cms energy.

Fig. 11 shows the pseudorapidity,

$$\eta = -\ln\tan(\theta/2), \tag{30}$$

of produced particles, excluding just the scattered electron. Both the ep and $e\pi$ distributions peak at $\eta = 3$; however, only the leading neutron shows a secondary peak for the produced nucleon at $\eta = 8$. Instead the ep distribution exhibits a broad shoulder in the proton direction. The beam pipe is located at $\eta = 4.0$, and it is clear that a large number of particles will escape undetected down the proton beam line. Any forward structure in the pseudorapidity distribution will remain unobserved.

The maximum pseudorapidity of produced particles, now excluding both the scattered electron and the leading neutron, is shown in Fig. 12. In the region accessible to measurement by experiments at HERA ($\eta_{max} < 4$), the distribution is falling exponentially with a slope of about 2.3. This result can be understood if we make the identification $\eta_{max} \sim \ln(1/z)$. Then $f_{\pi/p} \sim z$ implies an exponential fall with a slope of 2. In contrast, the pomeron P has $f_{\mathrm{P}/p} \sim 1/z$ [10] which implies a flat η_{max} distribution. The η_{max} distribution observed at HERA does have a flat tail[11]. This suggests that the large rapidity gap events, which are those in the flat tail, are predominantly due to pomeron exchange. Even to these events OPE will make a contribution, since the exchanged pion can scatter diffractively, that is via pomeron exchange, with a resulting rapidity gap.

There is very little neutral energy flow at small angles besides the neutron. Only 1% of the events have additional energy produced with $\theta < 0.5$ mr which might disturb the measurement of the leading neutron by accompanying it into a zero degree calorimeter. This energy flow, which consists mainly of photons from π^0 decay, peaks at 5 mr but is small on the average (Fig 13).

Also shown for comparison is the corresponding distribution for $ep \rightarrow eX$ which peaks at smaller angles and is slightly larger in magnitude.

6 Summary and Conclusions

HERA offers an extraordinary opportunity to examine target fragmentation in deep inelastic electron scattering experiments. In this paper we have concentrated on the window this opens for the study of the pion. An ep event with a leading n (or Δ) may be interpreted as virtual $e\pi$ scattering. The hadron-hadron scattering experiments reviewed above, suggest that 15%-20% of the ep events at HERA should be of this type. Every measurement made with the incoming proton as the assumed target can be duplicated with a virtual pion. Thus, in high Q^2 interactions the deep inelastic structure functions of the virtual pion can be measured for both charged and neutral currents, while $\gamma\pi$ collisions can be studied at low Q^2.

The tagging of a leading n or Δ will help clarify the role that nucleon charge exchange plays in the fragmentation of the target remnant. Also of particular interest is its role in low x electron-proton scattering. Saturation of the gluon density and gluon recombination could signal that coherence should play an important part in any discussion of shadowing and hot spots. How do such phenomena, predicted at HERA, interact with the 'restructuring' of the proton into a virtual pion and nucleon?

We remark also that $e\pi$ scattering at HERA presents an opportunity to explore electron scattering on both particle and antiparticle. Since both electrons and positrons are accelerated at HERA, the full set of $e^{\pm}\pi^{\pm}$ interactions are available for study.

Acknowledgments

I thank S. Bhadra, M. Derrick, D. Hanna, R. Klanner, E. Lohrmann, J. Martin, T. Massam, D. Stairs, and G. Wolf for their comments, suggestions and support. E. Gotsman, N. Nikolaev, A. Szczurek provided us with helpful insight on the theoretical aspects of one pion exchange. Dr. Massam's efforts greatly improved my understanding of the proton beam line at HERA and helped me considerably in the estimation of the acceptance for neutrons of

a zero degree calorimeter at ZEUS. I thank especially Gerd Hartner who provided the unpublished data from his thesis and its comparison to the predictions of one pion exchange.

References

* E-mail address: levman@physics.utoronto.ca

[1] J. D. Sullivan, Phys. Rev. **D5**, 1732 (1971).

[2] V. R. Zoller, Z. Phys. **C53**, 443 (1992).

[3] C. H. Llewellyn Smith, Phys. Lett. **B128**, 107 (1983).

[4] M. Ericson and A. W. Thomas, Phys. Lett. **B128**, 112 (1983).

[5] E. M. Henley and G. A. Miller, Phys. Lett. **B251**, 453 (1990).

[6] A. Szczurek and J. Speth, Nucl. Phys. **A555**, 249 (1993).

[7] S. Bhadra et al., Nucl. Instr. and Meth. **A354**, 479 (1995).

[8] ZEUS Collaboration, M. Derrick et al., *Initial study of leading neutrons in ep collisions at HERA*, ICHEP 94, in Glasgow, ref. 0692.

[9] G. Ingelman and P Schlein, Phys. Lett. **B152**, 256 (1985).

[10] P. Bruni, G. Ingelman and A. Solano, *Diffractively produced hadronic final states and the Pomeron structure*, in *Physics at HERA*, Vol. 1, W. Buchmüller and G. Ingelman, ed. (DESY, Notkestrasse 85, 2000 Hamburg 52, 1992) p. 363.

[11] ZEUS Coll., M. Derrick et al. Phys. Lett. **B315**, 481 (1993).

[12] G. Levman, *Is there pion exchange in large rapidity gaps at HERA?*, in *International Workshop on Deep Inelastic Scattering and Related Subjects*, Aharon Levy, ed. (World Scientific, Singapore, 1994) p. 373.

[13] H1 Coll., T. Ahmed et al, Phys. Lett. **B348**, 681 (1995).

[14] ZEUS Coll., M. Derrick et al., DESY 95-093 (1995).

[15] G. Marchesini et al., Comput. Phys. Commun. **67**, 465 (1992).

[16] R. D. Field and G. C. Fox, Nucl. Phys. **B80**, 367 (1974).

[17] S. N. Ganguli and D. P. Roy, Phys. Rep. **67**, 201 (1980).

[18] M. Bishari, Phys. Lett. **B38**, 510 (1972).

[19] J. Hanlon et al., Phys. Rev. Lett. **37**, 967 (1976).

[20] Gerd Hartner, *A study of pn interactions at 205 GeV/c*, Doctoral Thesis (McGill University, 1977), unpublished.

[21] P. D. B. Collins and A. D. Martin, *Hadron interactions*, (Adam Hilger Ltd., Bristol, 1984).

[22] J. Erwin et al., Phys. Rev. Lett. **35**, 980 (1975).

[23] N. N. Biswas et al., Phys. Rev. **D16**, 2090 (1977).

[24] P. D. Higgins et al., Phys. Rev. **D19**, 731 (1979).

[25] S. J. Barish et al., Phys. Rev. **D12**, 1260 (1975).

[26] F. T. Dao et al., Phys. Rev. Lett. **30**, 34 (1973).

[27] The cross section 1.04±0.10 mb obtained by[22] has $|t| < 0.88$ GeV^2 and has been adjusted upwards by 10±1% since the π^- and p induced cross sections have $|t| < 1$ GeV^2.

[28] The cross sections of the π^- energy compilation[24] have been averaged since there is no indication in the data of any energy dependence. The cubic background subtraction has been chosen.

[29] The cross sections of [19] and [20] have been averaged after the adjustment, described in the text, for the difference in t range.

[30] The cross sections obtained by [22], [25] and [26] have been averaged after adjustment for differences in t range.

[31] Jon Pumplin, Phys. Rev. **D8**, 2249 (1973).

[32] Jon Pumplin, Phys. Rev. **D7**, 795 (1973).

[33] H. Holtmann, G. Levman, N. N. Nikolaev, A. Szczczurek, and J. Speth, Phys. Lett. **B 338**, 1994 (363).

[34] B. Robinson et al., Phys. Rev. Lett. **34**, 1475 (1975).

[35] J. Engler et al., Nucl. Phys. **B64**, 173 (1973).

[36] J. Engler et al., Nucl. Phys. **B84**, 70 (1975).

[37] J. A. Campbell, R. B. Clark and D. Horn, Phys. Rev. **D2**, 217 (1970).

[38] K. J. M. Moriarty, J. H. Tabor and A. Ungkitchanukit, Phys. Rev. **D16**, 130 (1977).

[39] G. R. Goldstein and J. F. Owens, Nucl. Phys. **B118**, 29 (1977).

[40] W. S. C. Williams, *An introduction to elementary particles*, (Academic Press, New York, 1971).

[41] ZEUS Coll., M. Derrick et al., Phys. Lett. **B293**, 465 (1992).

[42] ZEUS Coll., M. Derrick et al., Z. Phys. **C63**, 391 (1994).

[43] ZEUS Coll., M. Derrick et al. Phys. Lett. **B297**, 404 (1992).

[44] T. H. Bauer, R. D. Spital, D. R. Yennie, and F. M. Pipkin, Rev. Mod. Phys. **50**, 262 (1978).

[45] A. Donnachie and P. V. Landshoff, Phys. Lett. **B296**, 227 (1992).

[46] J. F. Owens, Phys. Rev. **D30**, 943 (1984).

[47] J. Owens, Phys. Lett. **B266**, 126 (1991).

[48] E. Gotsman, Phys. Rev. **D9**, 1575 (1974).

[49] J. Bartels and J. Feltese, *QCD at low x: summary*, in *Physics at HERA*, Vol. 1, p. 131, W. Buchmüller and G. Ingelman, ed., (DESY, Notkestrasse 85, 2000 Hamburg 52, 1992).

[50] ZEUS Coll., *The ZEUS detector, status report, 1993*, Uwe Holm, ed., (DESY, Notkestrasse 85, 2000 Hamburg 52, 1993).

[51] We thank G. Wolf who pointed out to us the possibility of studying $n \to p$ with a deuteron beam and a leading proton spectrometer, and M. Derrick who stressed to us the importance of a forward neutron calorimeter as a tag for spectator neutrons.

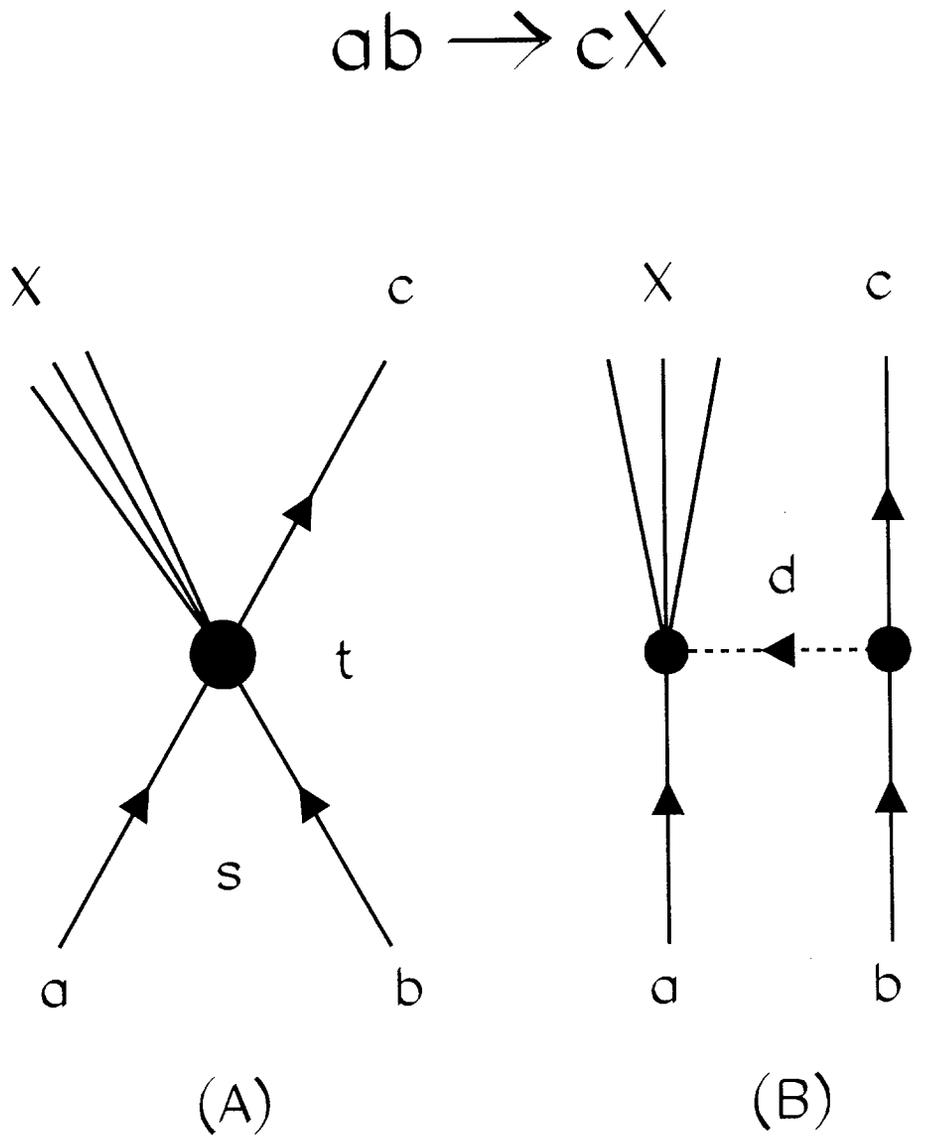

Figure 1: (A) shows the Mandelstam diagram for the single particle inclusive reaction $ab \to cX$; (B) is the corresponding diagram assuming factorization and the exchange of a virtual particle d.

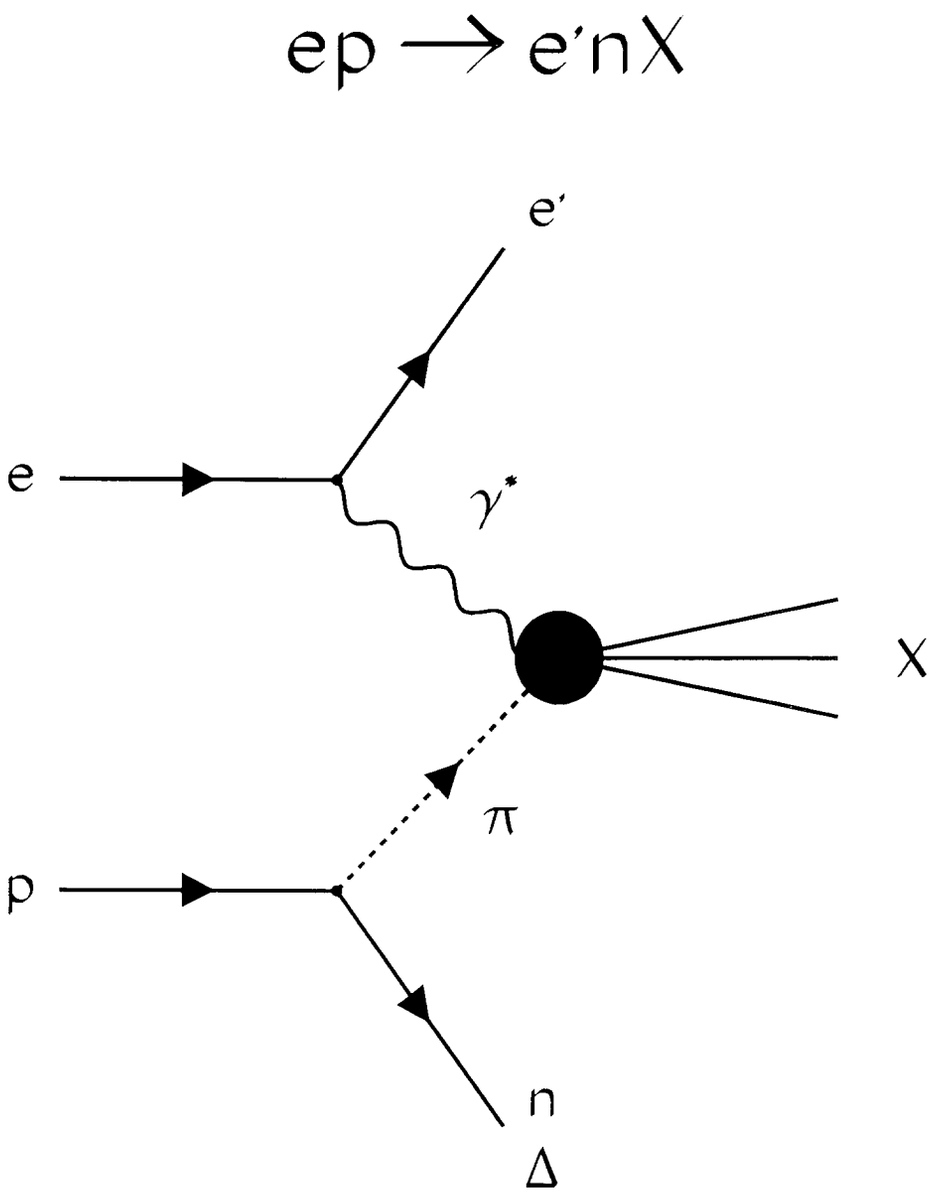

Figure 2: Diagram for the two particle inclusive reaction $ep \rightarrow e'[n, \Delta]X$ where the $\gamma^* p$ vertex is assumed to factorize and be dominated by π exchange.

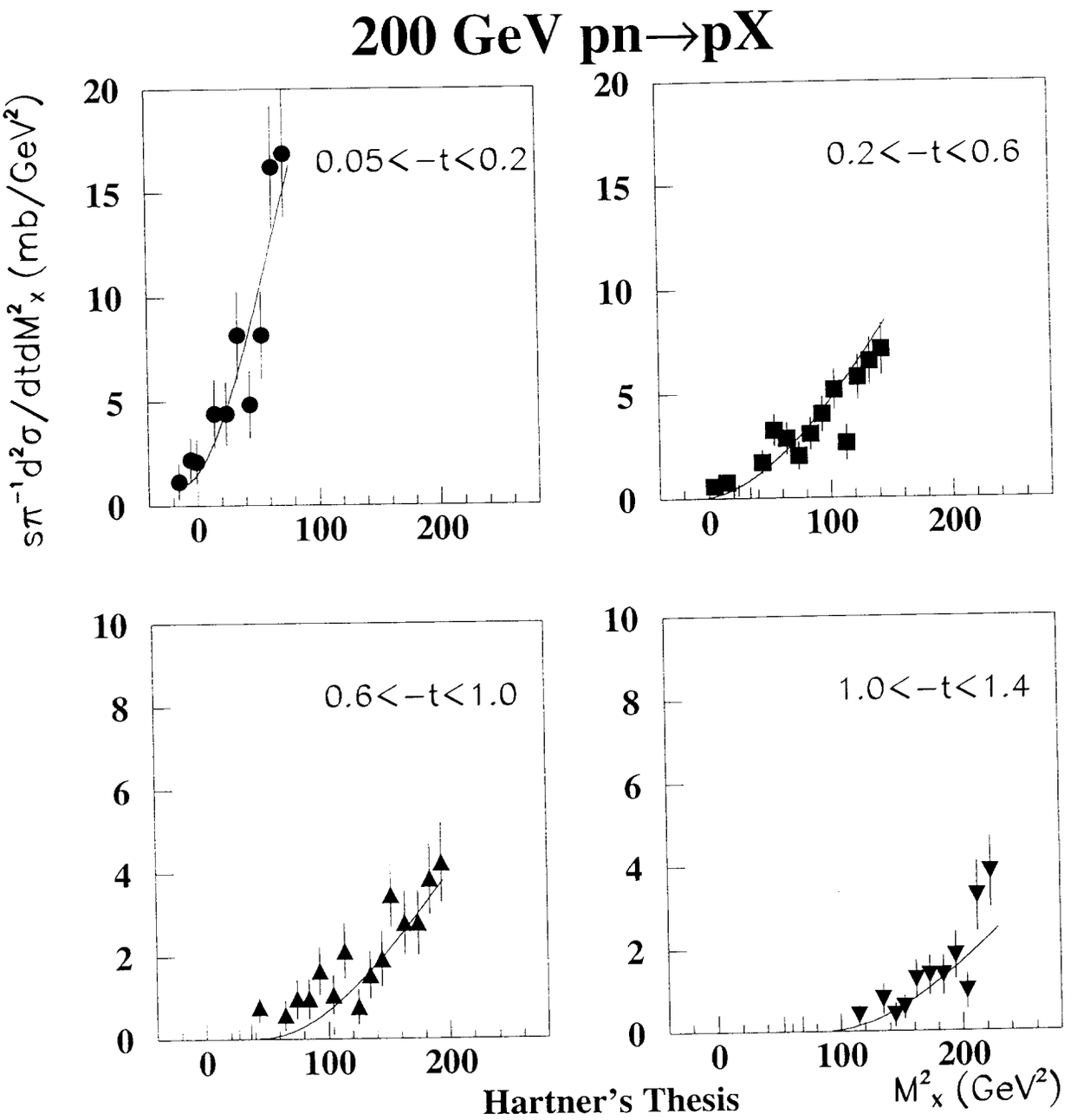

Figure 3: The invariant cross sections for $pn \to pX$ at 200 GeV in bins of t. The curve is the prediction of the OPE formula with the pion trajectory retained and the form factor omitted.

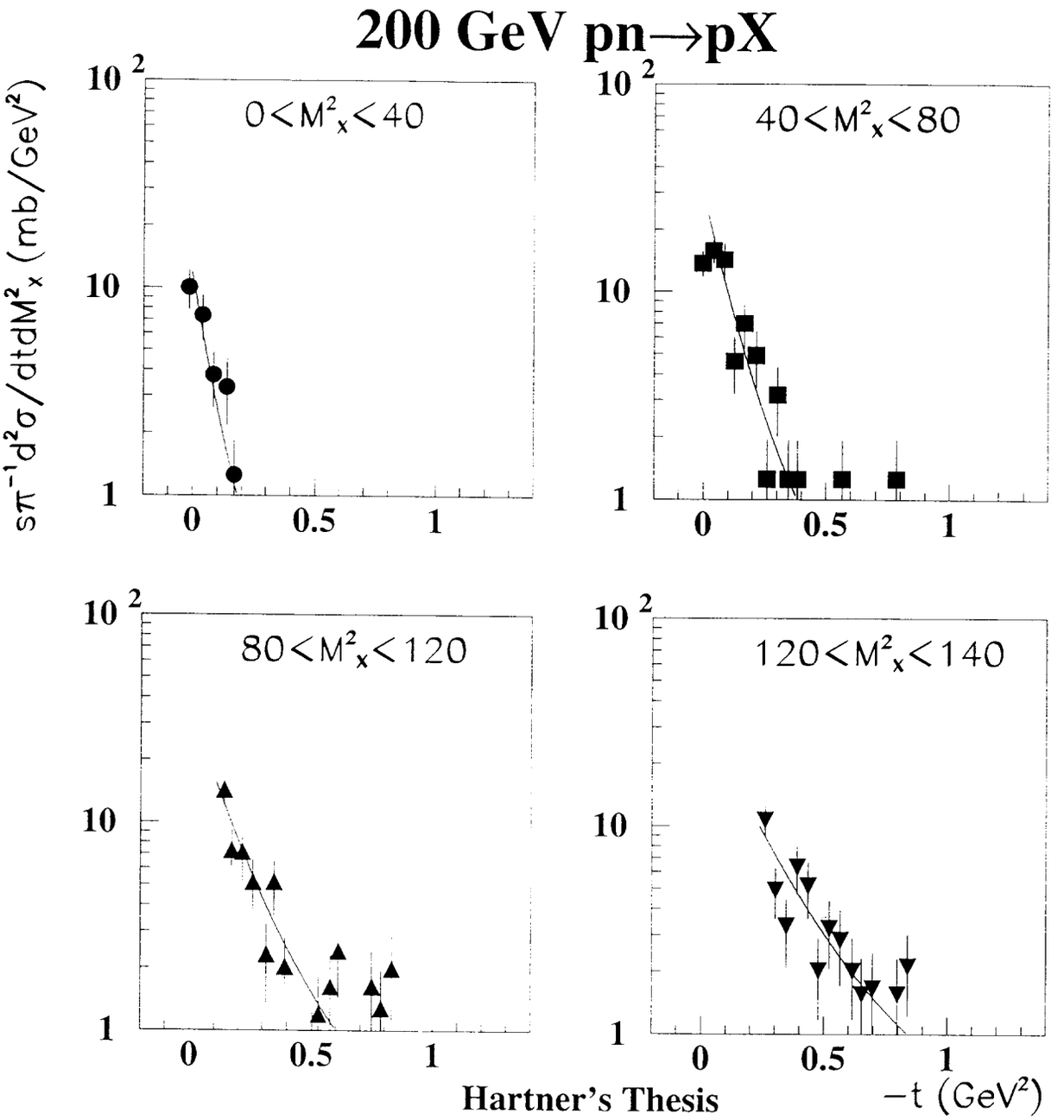

Figure 4: The invariant cross sections for $pn \to pX$ at 200 GeV in bins of M_X^2. The curve is the prediction of the OPE formula with the pion trajectory retained and the form factor omitted.

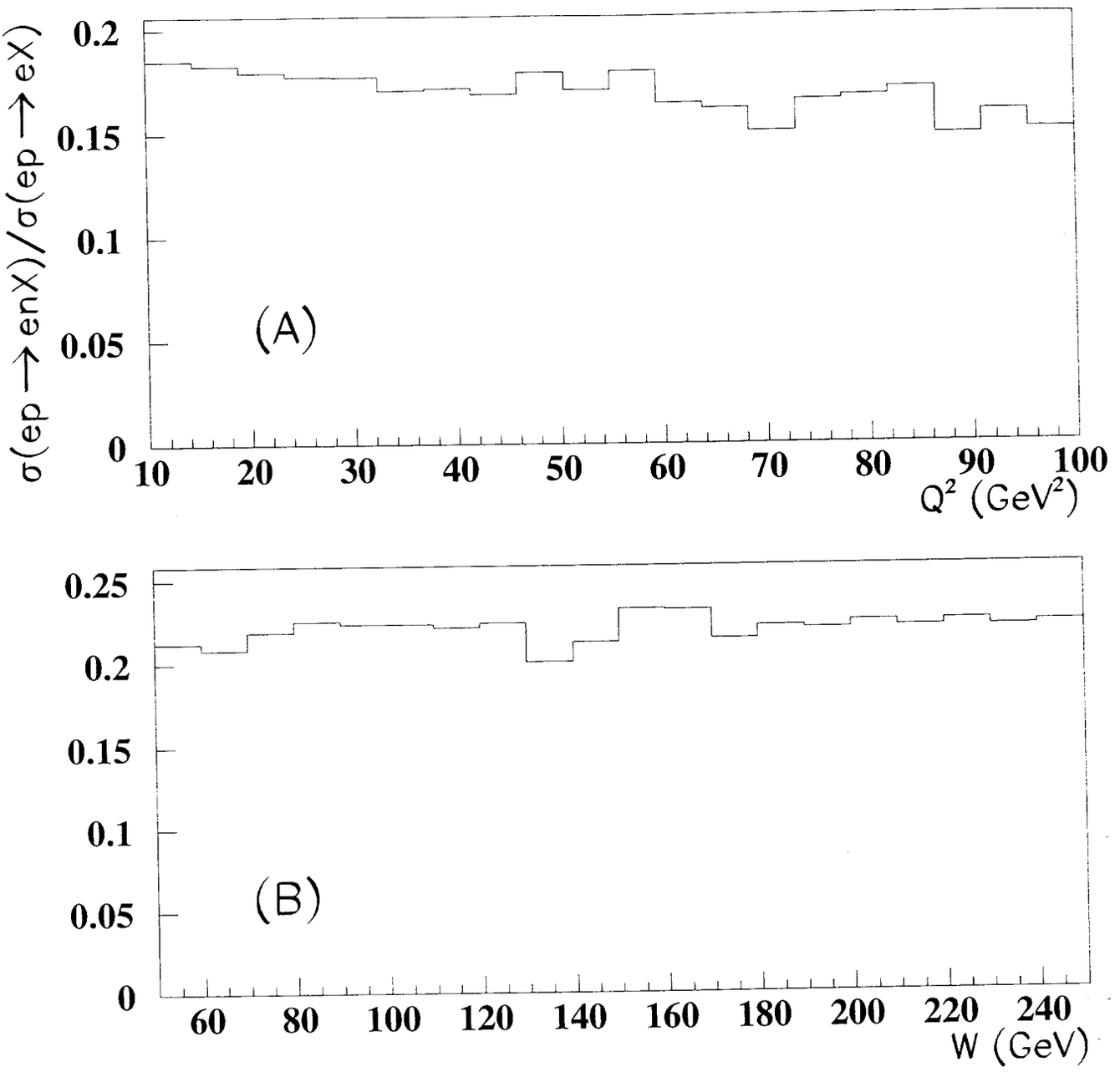

Figure 5: The ratio of leading neutron events to ordinary DIS events as a function of (A) Q^2 and (B) W.

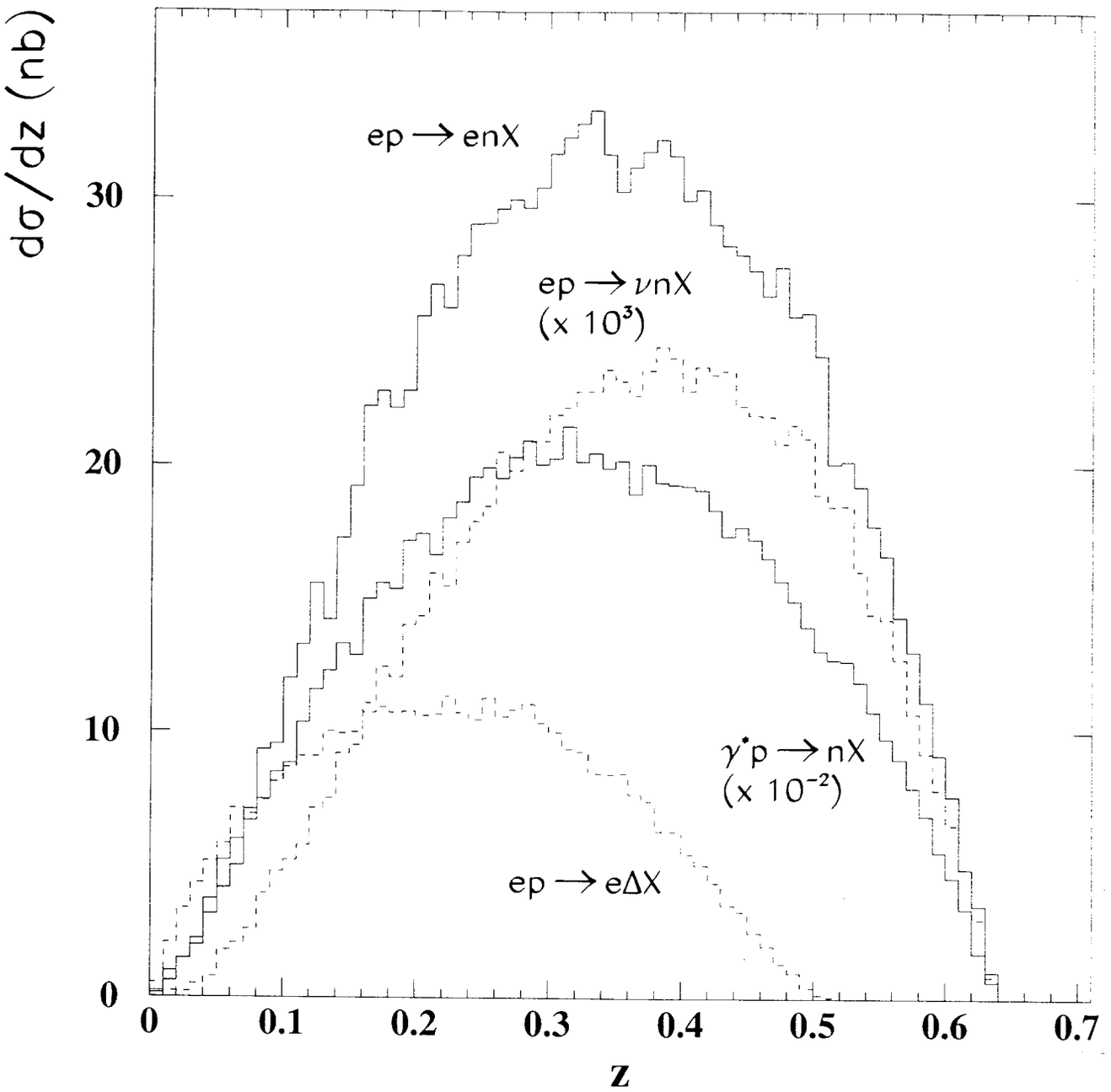

Figure 6: The z distribution of n and Δ. The Δ is normalized in the ratio 1:3.5 relative to the neutron. The charged current distribution has been multiplied by 10^3 and the photoproduction distribution by 10^{-2}. For DIS $Q^2 > 10$ GeV^2. For photoproduction $0.2 < y < 0.8$.

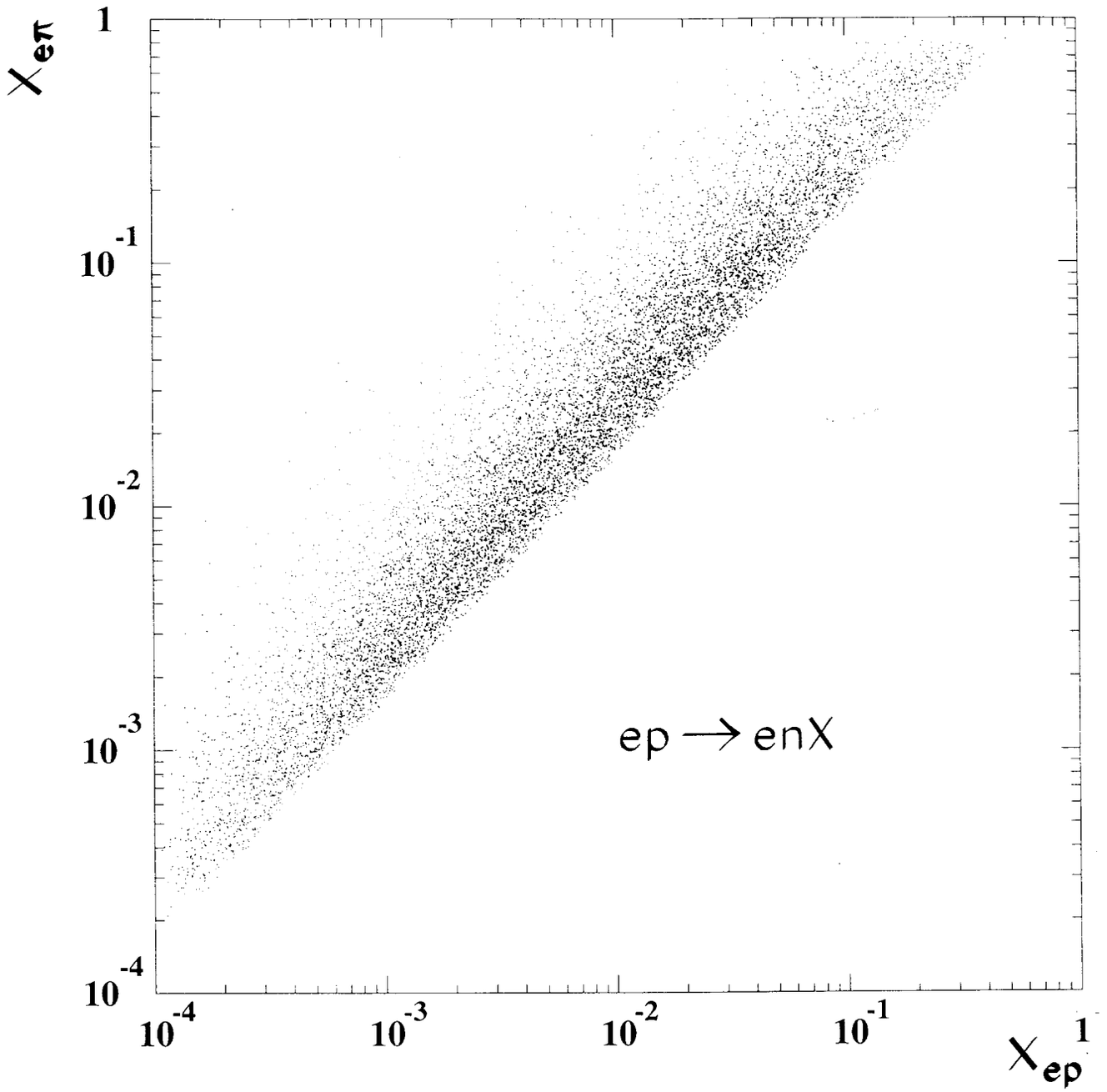

Figure 7: A scatter plot for $Q^2 > 10$ GeV^2 of $x_{ep} = x_{BJ}$, the struck parton's momentum fraction for ep scattering versus $x_{e\pi} = x_{BJ}/z$, the parton's momentum fraction for virtual $e\pi$ scattering tagged with a leading neutron.

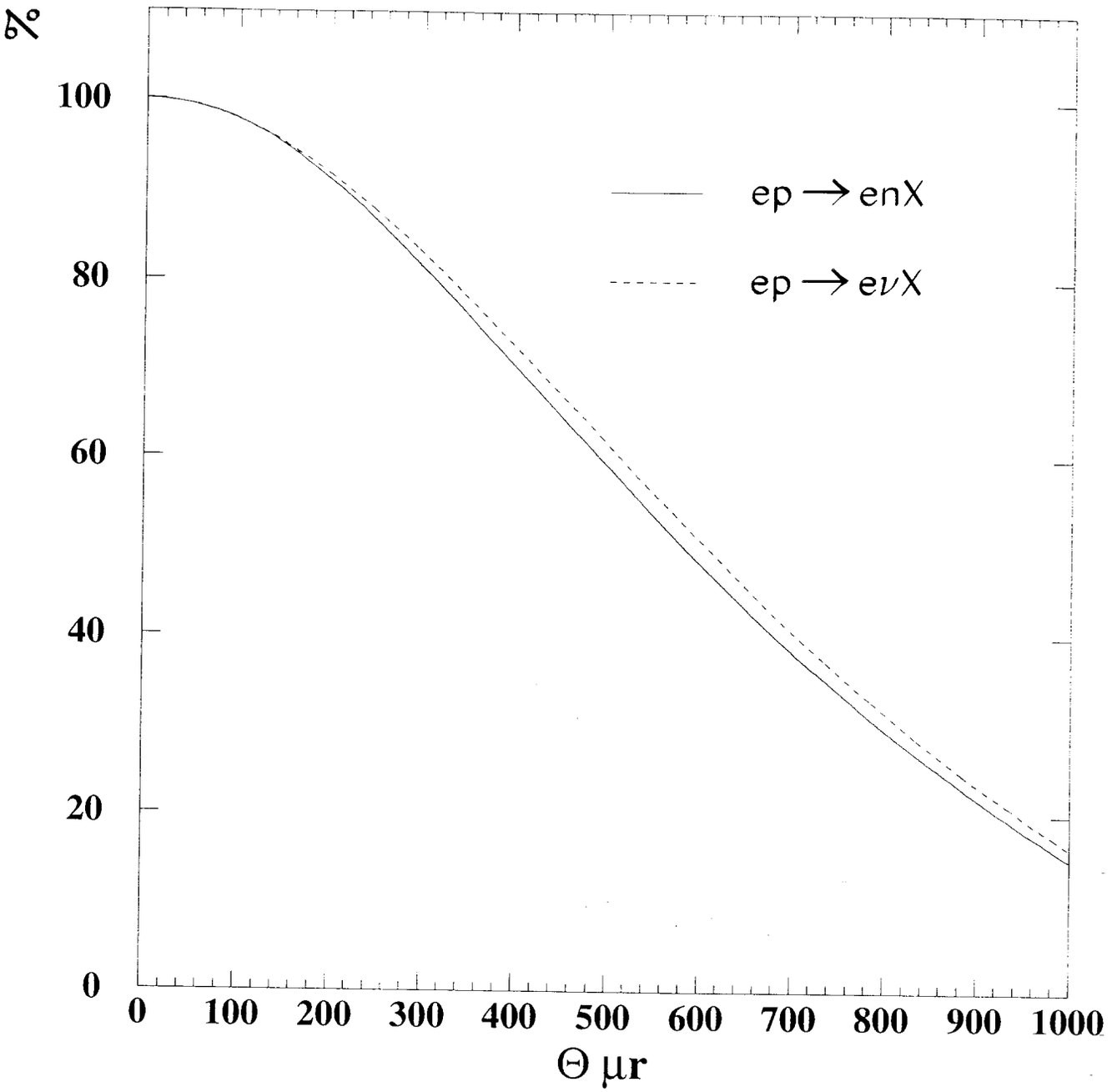

Figure 8: The integrated production angle spectrum of the leading neutron: the percentage of neutrons produced with scattering angle greater than θ_n.

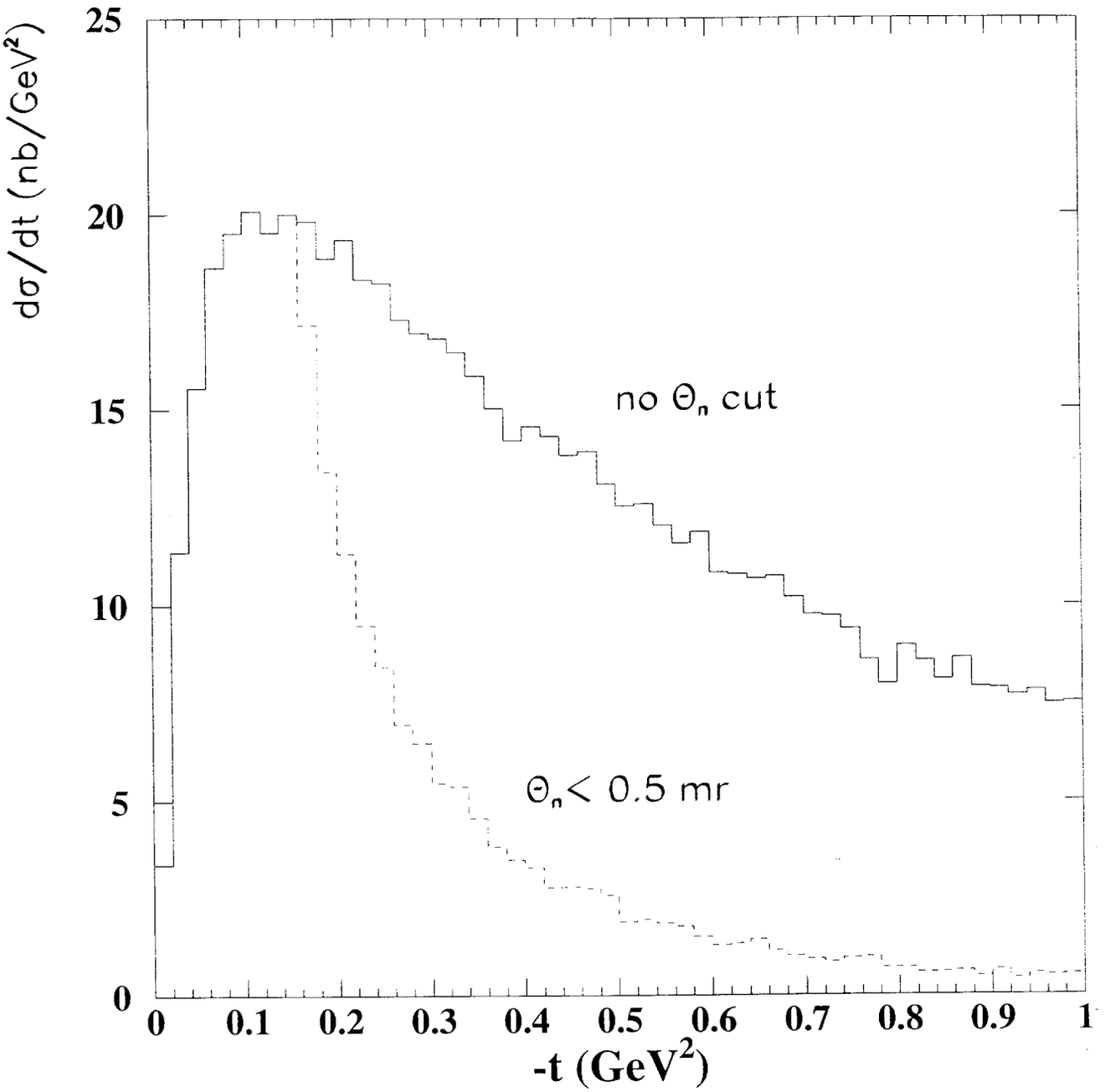

Figure 9: The t distribution for leading neutrons in neutral current DIS events with $Q^2 > 10$ GeV^2. It is also shown with the requirement that the angle of the neutron satisfy $\theta_n < 0.5$ mr.

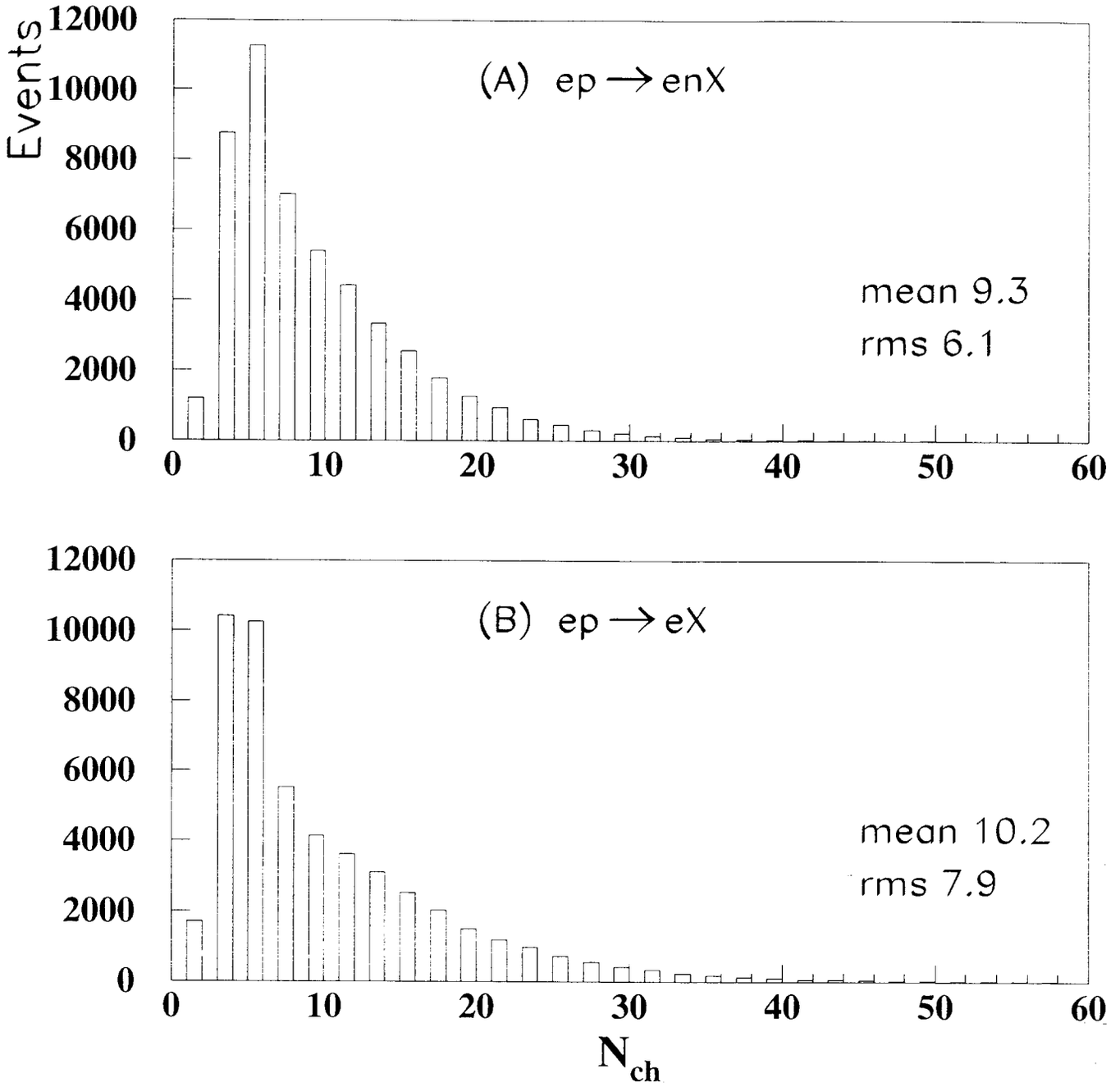

Figure 10: The charged multiplicity distribution for (A) leading neutron events and (B) ordinary DIS events.

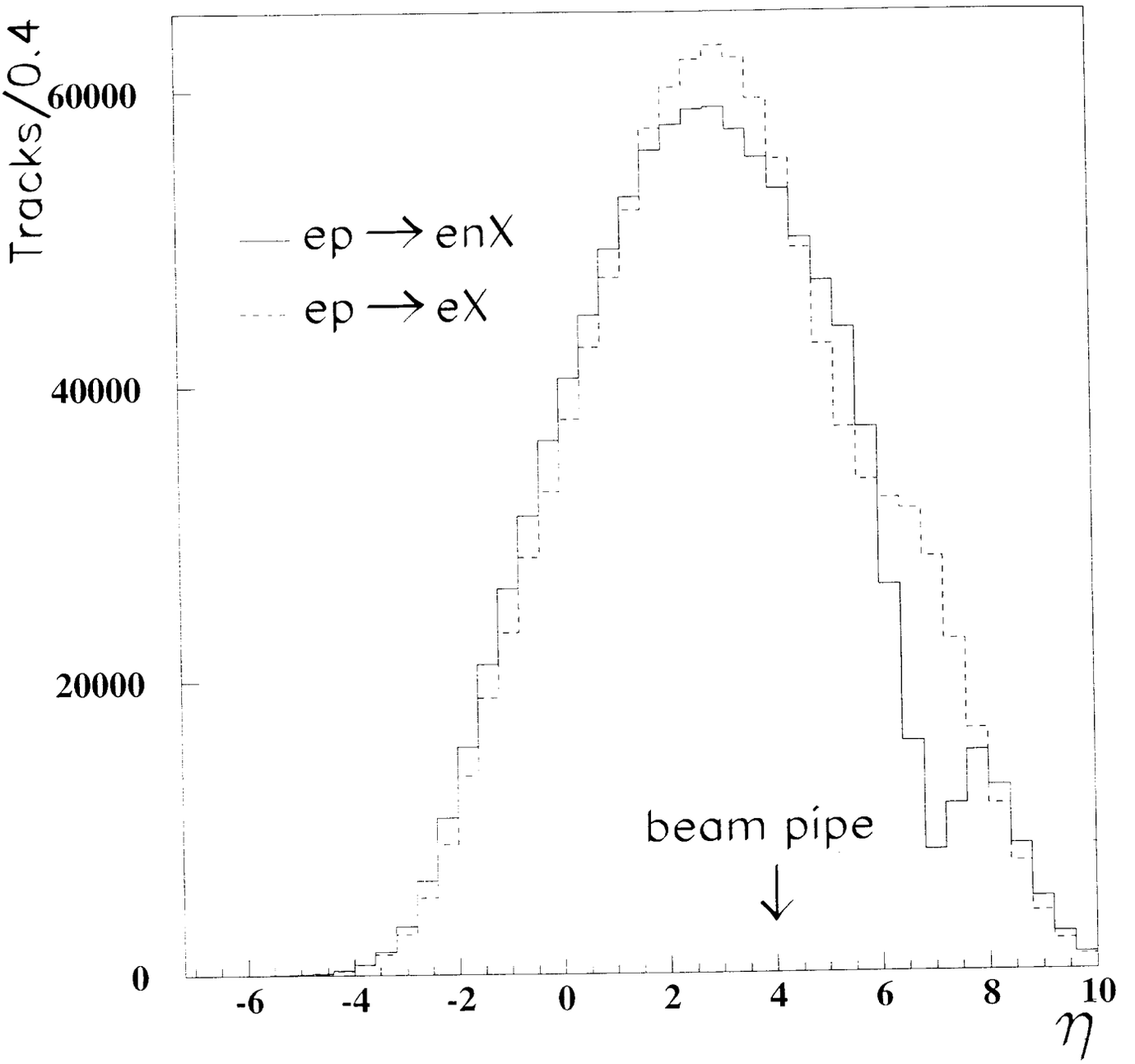

Figure 11: The distribution of pseudorapidity $\eta = -\ln\tan(\theta/2)$ of all particles for the reactions $ep \to enX$ and $ep \to eX$.

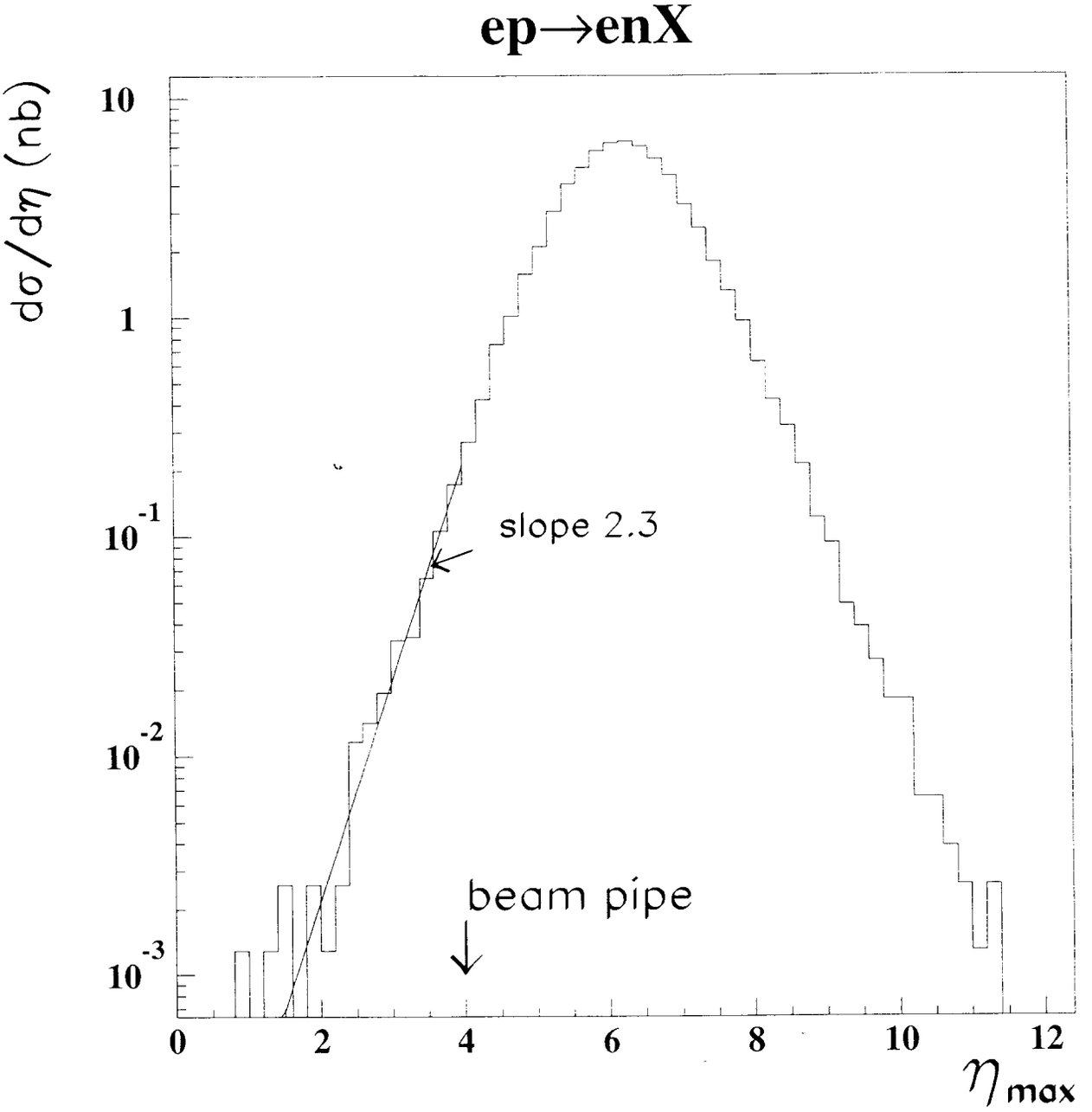

Figure 12: The η_{max} distribution for $ep \rightarrow enX$ events. The curve is an exponential fit to the distribution for $\eta_{max} < 4$, the observable region in the ZEUS and H1 experiments.

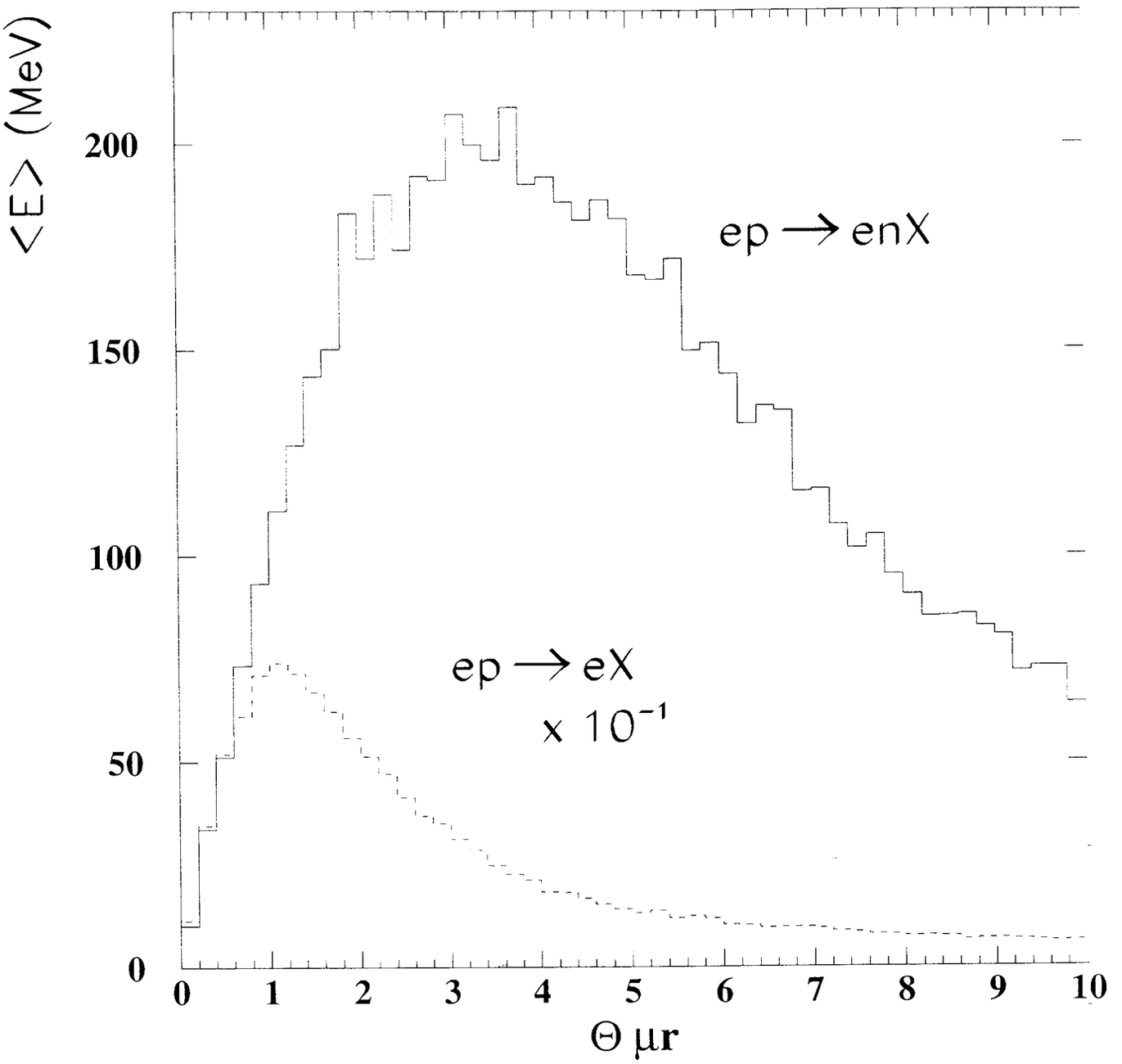

Figure 13: The average neutral energy flow per event $< E >$ near zero degrees in the proton direction. The leading neutron has been removed. The distribution for $ep \rightarrow eX$ has been divided by 10.